ARTICLE NO. 78-1213R

Numerical Procedure for the Computation of Irrotational Conical Flows

B. Grossman*
Grumman Aerospace Corporation, Bethpage, N.Y.

A numerical procedure has been developed for the computation of steady inviscid supersonic flow about general conical bodies at incidence. The method is based on solutions of the exact nonlinear potential equation in an orthogonal coordinate system generated through a stereographic projection and standard conformal mapping techniques. Accurate numerical solutions are obtained through the application of mixed-flow relaxation procedures. Results are presented for a wide variety of configurations from slender cones to thin wings with blunt leading edges, and are compared with existing theories and experimental data. Some interesting results have been obtained depicting the "lift-off" of the vortical singularity on elliptic cones at high angles of attack.

I. Introduction

THE study of conical flows has provided a means to infer important effects on three-dimensional supersonic flow past wings and bodies, dating back to the work of Busemann in the early 1930's and 1940's. In these flowfields, all fluid properties remain constant along straight lines (rays) emanating from a specific point, the apex. Thus, the dependent variables will be functions of the two independent coordinates describing the rays.

Much of the early theoretical work on conical flows is based on a variety of linearizing assumptions. These, for the most part, fall into the following categories: linearized theory,[1-3] slender body theory,[4-6] second-order slender body theory,[7] not so slender body theory,[8] and other variants; and recently the complete first-order linearized solution for elliptic cones.[9] The lower-order methods are generally easy to apply to a wide variety of configurations and conditions. However, they do not provide accurate solutions in many important cases of interest. The higher-order methods have improved accuracy but are cumbersome and significantly less general. All of these methods fail for flows with embedded shock waves and for cases where there are blunt supersonic or sonic leading edges. Lighthill[10] and Frohn[11] have developed uniformly valid solutions that predict embedded shock waves in some special cases.

For many problems of aerodynamic interest there is no recourse but to consider nonlinear conical flows; i.e., consider flows with arbitrary, thin cross sections, blunt leading edges, low to moderate supersonic Mach numbers, and moderate incidence. Certainly, there have been a variety of attempts to perform theoretical studies of nonlinear conical flows, such as those discussed by Bulakh.[12] None of these, however, has been successful in developing general solutions, as mentioned earlier.

Early attempts at numerical conical flow solutions included linearized circular cones at small incidence,[13-15] inverse methods,[16] and distance-asymptotic methods.[17,18] Some accurate solutions for circular and elliptic cones at angles of attack on the order of the cone half angle have been obtained by Jones[19] and Klunker et al.[20] using the method of lines.

More recent attempts at general, nonlinear conical flow solutions involve finite-difference solutions of Euler's equations by marching or relaxation procedures. The marching methods with explicit shock fitting include the work by Moretti and Pandolfi[21] for simple cones and low incidence and the extension by Marconi and Siclari[22] to more general configurations at moderate incidence. The relaxation methods include the work by Kutler[23] using shock capturing and by Daywitt et al.[24] with floating shock fitting on circular cones at high incidence. (A more detailed survey of the various numerical procedures available for circular cones appears in Ref. 24.) Of these methods, the work of Marconi and Siclari appears to attack successfully the general problem of nonlinear conical flow on arbitrary geometries. The principal drawbacks seem to be primarily due to the large computer times necessary to obtain convergence. Other difficulties are related to the numerical treatment of the vortical singularity on the leeward surface and to the choice of the axial marching direction. The latter restricts the computation to the conditions of $M_\infty > 1.7$ for most sweepback angles of practical aerodynamic interest.

At large angles of incidence, conical flow problems develop two fundamental difficulties which prevent a straightforward numerical solution. First, as the angle of attack is increased, the crossflow velocity will accelerate to a supersonic value as the flow passes around the leading edge or shoulder of the cone. This changes the nature of the governing partial differential equations from elliptic to a mixed elliptic-hyperbolic type and results in the appearance of an embedded shock wave on the leeward surface of the cone. Another difficulty arises due to the nature of the nodal singularity at the conical stagnation point on the leeward generator of the cone. (At a conical stagnation point, the velocity vector contains only a single component in the direction of a ray and the crossflow velocity will thus be zero.) At the vortical singularity the entropy, density and radial velocity component are multivalued. As the angle of attack further increases, the conical stagnation point lifts off the leeward surface of the cone. The nature of this singularity has been discussed by Ferri[15] and later in more detail by Melnik,[25] among others. Detailed numerical calculations of crossflow streamlines, including "lift-off," have been performed by Bakker and Bannink[26] for very slender circular cones using linearized theory. An approach using a modified method of lines by

Presented as Paper 78-1213 at the AIAA 11th Fluid and Plasma Dynamics Conference, Seattle, Wash., July 10-12, 1978; submitted Aug. 25, 1978; revision received Feb. 8, 1979.

Index categories: Supersonic and Hypersonic Flow; Computational Methods.

*Head, Theoretical Aerodynamics Laboratory, Research Dept. Member AIAA.

Fletcher[27] has computed details of the vortical singularity on a circular cone at high supersonic Mach numbers. Finite-difference solutions[24] have not yet been able to give adequate resolution to the "lift-off" phenomenon.

The present work attempts to develop an accurate, efficient numerical procedure for the computation of the steady, inviscid supersonic flow over general conical bodies at moderate supersonic Mach numbers (of the order $1.2<M_\infty<2.5$ for wings of aerodynamic interest), over a complete range of angles of attack. The geometries range from blunt cones to very thin delta wings with arbitrary, smooth thickness and camber distributions. In order to facilitate our solution, we make the additional assumption of irrotational flow and, hence, neglect all entropy variations. This restriction should provide accurate results provided that the Mach number normal to all shock waves be less than ~ 1.4. The irrotational flow assumption retains all of the important nonlinear features of the flowfield and furthermore, the formulation of the problem in the crossflow plane has the salient mathematical properties of two-dimensional transonic potential flow. Thus, we are able to draw upon the highly successful methods developed for solving the nonlinear, mixed elliptic-hyperbolic potential equation in transonic flow.[28-30] In addition, since the method will apply to very thin wings, where high levels of accuracy are necessary at the leading edges, the use of general conformal mapping methods becomes invaluable. However, a preliminary mapping of the surface of a sphere to a geometrically conformal surface is advantageous to the development of an appropriate orthogonal curvilinear coordinate system.

Details of the various coordinate transformations and mappings are presented in Sec. II of this report. A derivation of the nonlinear potential flow equations and boundary conditions appears in Sec. III, followed by a discussion of the numerical formulation of the boundary-value problem in Sec. IV. Results are presented for a wide variety of geometries and flow conditions in Sec. V. A large number of cases are presented in order to substantiate the method by comparison with existing methods and available wind-tunnel data. A number of crossflow streamline patterns will be shown indicating the "lift-off" of the vortical singularity at high angles of attack on circular and elliptic cones.

II. Coordinate Transformations

The natural coordinate system for conical flows is spherical coordinates (r,ψ,ω) shown in Fig. 1 and related to the Cartesian coordinates (x,y,z) by

$$x=r\cos\omega\sin\psi, \quad y=r\sin\omega\sin\psi, \quad z=r\cos\psi \tag{1}$$

The axis of the cone lies along the z axis ($\psi=0$). A conical body is simply defined in this coordinate frame as $\psi=f(\omega)$ on the surface of the sphere; $r=$ constant.

Since we intend to solve the exact potential equation with exact boundary conditions on relatively general conical bodies, it would be desirable to generate a transformed domain where the mapped body surface is a coordinate line. In two-dimensional flows this is conveniently handled through conformal mapping methods (e.g., Ives[31]). However, on the surface of the sphere, it is first necessary to transform the spherical coordinates (ψ,ω) to a surface (p,q) which is conformal (in the terminology of Weatherburn[32]). The differential arc length ds on this surface is represented by

$$ds^2=r^2(d\psi^2+\sin^2\psi d\omega^2)=k^2(dp^2+dq^2) \tag{2}$$

A convenient transformation of this type which has been utilized by cartographers, is the sterographic projection (i.e., Weatherburn[32]), where

$$p+iq=\tan(\psi/2)e^{i\omega} \tag{3}$$

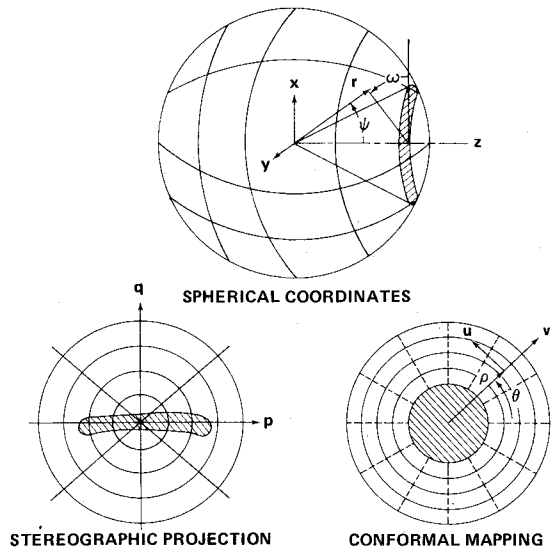

Fig. 1 Sequence of mappings.

Under this transformation, we have

$$ds^2=r^2\frac{\sin^2\psi}{\tan^2(\psi/2)}(dp^2+dq^2) \tag{4}$$

Now in the pq plane meridians on the sphere are represented by straight lines through the origin and parallels of latitude by concentric circles as illustrated in Fig. 1.

After applying the sterographic projection, the surface of the sphere becomes "conformal" as verified by Eq. (4), and we can then further map our arbitrary geometry using standard conformal mapping procedures. In particular, for conical bodies of approximate elliptic cross section, the application of a Joukowski mapping will produce a nearly circular image. Thus, for this case

$$\frac{S-S_0}{S+\bar{S}_0}=\left(\frac{\gamma-S_0/2}{\gamma+\bar{S}_0/2}\right)^2 \tag{5}$$

where

$$\gamma=\rho e^{i\theta}, \quad S=p+iq \tag{6}$$

and S_0 is the location of the singularity in the pq plane. S_0 is normally chosen to be located halfway between the center of maximum curvature and the leading edge.

The mapped domain, consisting of the orthogonal curvilinear coordinates, (ρ,θ,R), where $R=r$, forms the basis of the computation. The surface of the cone is represented as

$$\rho=b(\theta) \tag{7}$$

It is convenient to introduce here the metrics of the mapping h_ρ, h_θ, h_R which will be used in the derivation of the governing equations

$$h_\rho=\left[\left(\frac{\partial x}{\partial\rho}\right)^2+\left(\frac{\partial y}{\partial\rho}\right)^2+\left(\frac{\partial z}{\partial\rho}\right)^2\right]^{1/2}=RH(\rho,\theta) \tag{8a}$$

$$h_\theta=\left[\left(\frac{\partial x}{\partial\theta}\right)^2+\left(\frac{\partial y}{\partial\theta}\right)^2+\left(\frac{\partial z}{\partial\theta}\right)^2\right]^{1/2}=\rho RH(\rho,\theta) \tag{8b}$$

$$h_R=\left[\left(\frac{\partial x}{\partial R}\right)^2+\left(\frac{\partial y}{\partial R}\right)^2+\left(\frac{\partial z}{\partial R}\right)^2\right]^{1/2}=1 \tag{8c}$$

where

$$H=\frac{\sin\psi}{(p^2+q^2)^{1/2}}\,h(\rho,\theta) \tag{9}$$

and h is the metric of the conformal mapping

$$h=\left|\frac{\mathrm{d}S}{\mathrm{d}\gamma}\right|=\left|\frac{(S-S_0)(S+\bar{S}_0)}{(\gamma-S_0/2)(\gamma+\bar{S}_0/2)}\right| \tag{10}$$

In addition, the numerical computation will be performed in a domain where the body surface is a coordinate line. To achieve this we use a simple "shearing" transformation

$$X=\theta,\quad Y=\frac{\rho-b(\theta)}{c(\theta)-b(\theta)},\quad Z=R \tag{11}$$

where $c(\theta)$ is the position of the outer boundary of computation. As discussed in the following sections $c(\theta)$ is chosen so that it is located outside the bow wave.

III. Governing Equations and Boundary Conditions

For irrotational flow, the governing inviscid steady flow equations in terms of the velocity vector $\bar{Q}$ and the speed of sound, a, may be written as

$$a^2\nabla\cdot\bar{Q}-\tfrac{1}{2}\bar{Q}\cdot\nabla(\bar{Q}\cdot\bar{Q})=0 \tag{12}$$

and

$$a^2+\frac{\gamma-1}{2}\bar{Q}\cdot\bar{Q}=a_0^2 \tag{13}$$

where a_0 is the stagnation speed of sound and γ is the ratio of specific heats. We introduce a perturbation potential ϕ such that

$$\bar{Q}=\nabla\phi+\bar{q}_\infty \tag{14}$$

where the freestream velocity vector $\bar{q}_\infty$ may be written in terms of the original Cartesian coordinates x, y, z with unit vectors $\hat{i}$, $\hat{j}$, $\hat{k}$ and angle of attack α as

$$\bar{q}_\infty=\sin\alpha\hat{j}+\cos\alpha\hat{k} \tag{15}$$

Under the assumption of conical flow it can be shown that the potential is of the form

$$\phi=RF(\rho,\theta) \tag{16}$$

and the perturbation velocity components in the ρ, θ, and R directions are

$$\bar{q}=\nabla\phi=v\hat{i}_\rho+u\hat{i}_\theta+w\hat{i}_R=\frac{1}{H}\frac{\partial F}{\partial\rho}\hat{i}_\rho+\frac{1}{\rho H}\frac{\partial F}{\partial\theta}\hat{i}_\theta+F\hat{i}_R \tag{17}$$

where the metric of the mapping H is defined in Eq. (9). The complete velocity vector is written as

$$\begin{aligned}\bar{Q}&=\bar{q}+\bar{q}_\infty=(v+v_\infty)\hat{i}_\rho+(u+u_\infty)\hat{i}_\theta+(w+w_\infty)\hat{i}_R\\&=V\hat{i}_\rho+U\hat{i}_\theta+W\hat{i}_R\end{aligned} \tag{18}$$

where

$$v_\infty(\rho,\theta)=\frac{1}{H}\left[\sin\alpha\left(\cos\psi\sin\omega\frac{\partial\psi}{\partial\rho}-\cos\omega\frac{1}{\rho}\frac{\partial\psi}{\partial\theta}\right)-\cos\alpha\sin\psi\frac{\partial\psi}{\partial\rho}\right] \tag{19a}$$

$$u_\infty(\rho,\theta)=\frac{1}{H}\left[\sin\alpha\left(\cos\psi\sin\omega\frac{1}{\rho}\frac{\partial\psi}{\partial\theta}+\cos\omega\frac{\partial\psi}{\partial\rho}\right)-\cos\alpha\sin\psi\frac{1}{\rho}\frac{\partial\psi}{\partial\theta}\right] \tag{19b}$$

$$w_\infty(\rho,\theta)=\sin\alpha\sin\psi\sin\omega+\cos\alpha\cos\psi \tag{19c}$$

with $\psi,\omega,(\partial\psi/\partial\rho)$, and $(\partial\psi/\partial\theta)$ related to ρ,θ through Eqs. (3, 5, and 6).

Introducing the conical potential F through Eqs. (14-19) into the governing Eqs. (12) and (13) and performing the vector differentiations using the rules for orthogonal curvilinear coordinates ultimately yields

$$\begin{aligned}0&=(a^2-V^2)\frac{\partial^2F}{\partial\rho^2}-\frac{2}{\rho}UV\left(\frac{\partial^2F}{\partial\rho\partial\theta}-\frac{1}{\rho}\frac{\partial F}{\partial\theta}\right)\\&+(a^2-U^2)\left(\frac{1}{\rho^2}\frac{\partial^2F}{\partial\theta^2}+\frac{1}{\rho}\frac{\partial F}{\partial\rho}\right)+H^2F(2a^2-V^2-U^2)\\&+(V^2-U^2)\left(v\frac{\partial H}{\partial\rho}-\frac{u}{\rho}\frac{\partial H}{\partial\theta}\right)+2UV\left(u\frac{\partial H}{\partial\rho}+\frac{v}{\rho}\frac{\partial H}{\partial\theta}\right)\end{aligned} \tag{20}$$

and

$$a^2=a_0^2-\frac{\gamma-1}{2}(V^2+U^2+W^2) \tag{21}$$

where

$$V=\frac{1}{H}\frac{\partial F}{\partial\rho}+v_\infty(\rho,\theta) \tag{22a}$$

$$U=\frac{1}{\rho H}\frac{\partial F}{\partial\theta}+u_\infty(\rho,\theta) \tag{22b}$$

$$W=F+w_\infty(\rho,\theta) \tag{22c}$$

The preceding governing equations for the reduced conical potential $F(\rho,\theta)$ in the mapped domain, are independent of the spherical radius R, and the terms involving the second derivatives of F are of the identical form as the two-dimensional transonic full potential equation. The three dimensionality of the flow is principally contained in the term proportional to F. These equations are of mixed type, being elliptic when the crossflow velocity magnitude $Q_c=\sqrt{U^2+V^2}$ is less than a and hyperbolic when $Q_c>a$. Since Q_c must necessarily be zero on the body at the symmetry plane, it is to be expected that if the crossflow becomes supersonic it will terminate in an embedded shock wave.

The boundary condition on the surface of the body is the vanishing of the normal velocity. This condition is

$$V=\frac{1}{b}\left(\frac{\mathrm{d}b}{\mathrm{d}\theta}\right)U$$

or

$$\frac{1}{H}\frac{\partial F}{\partial\rho}+v_\infty=\frac{1}{b}\left(\frac{\mathrm{d}b}{\mathrm{d}\theta}\right)\left[\frac{1}{\rho H}\frac{\partial F}{\partial\theta}+u_\infty\right] \tag{23}$$

on $\rho=b(\theta)$. At the symmetry planes $\omega=\pm\pi/2$, the normal velocity U must vanish and since $u_\infty(\rho,\pm\pi/2)$ is zero

$$\frac{\partial F(\rho,\pm\pi/2)}{\partial\theta}=0 \tag{24}$$

(An extension of the method to account for both sideslip and incidence could easily be obtained by replacing the preceding symmetry property with a condition of periodicity.) In the far field, outside the bow wave, the perturbation potential and its first derivatives must vanish

$$F,\ \frac{\partial F}{\partial \rho},\ \frac{\partial F}{\partial \theta} \to 0 \text{ outside the bow wave} \tag{25}$$

The implementation of the far-field boundary condition will be discussed in the next section.

In the development of the numerical solution to Eqs. (20) and (21) we utilize the additional shearing transformation given by Eqs. (11). The governing equations then become

$$A_1\frac{\partial^2 F}{\partial X^2}+A_2\frac{\partial^2 F}{\partial X\partial Y}+A_3\frac{\partial^2 F}{\partial Y^2}+A_4\frac{\partial F}{\partial X}+A_5\frac{\partial F}{\partial Y}+A_6F+A_7=0 \tag{26}$$

where

$$A_1=(a^2-U^2)\frac{1}{\rho^2}$$

$$A_2=-2UV\frac{1}{\rho}Y_\rho+2(a^2-U^2)\frac{1}{\rho^2}Y_\theta$$

$$A_3=(a^2-V^2)Y_\rho^2-2UV\frac{1}{\rho}Y_\rho Y_\theta+(a^2-U^2)\frac{1}{\rho^2}Y_\theta^2$$

$$A_4=2UV\frac{1}{\rho^2}$$

$$A_5=-2UV\frac{1}{\rho}\left(Y_{\rho\theta}-\frac{1}{\rho}Y_\theta\right)+(a^2-U^2)\frac{1}{\rho}\left(\frac{1}{\rho}Y_{\theta\theta}+Y_\rho\right)$$

$$A_6=H^2(2a^2-V^2-U^2)$$

$$A_7=(V^2-U^2)[vY_\rho H_Y-u\frac{1}{\rho}(H_X+Y_\theta H_Y)]$$

$$+2UV[uY_\rho H_Y+v\frac{1}{\rho}(H_X+Y_\theta H_Y)]$$

and

$$v=\frac{1}{H}Y_\rho F_Y,\quad u=\frac{1}{\rho H}(F_X+Y_\theta F_Y)$$

$$V=v+v_\infty,\quad U=u+u_\infty,\quad W=F+w_\infty$$

In order to utilize Jameson's rotated difference scheme,[30] we need the principal part of Eq. (26) written in suitable form. To achieve this, we define, in the crossflow plane, the local streamline direction s and the direction normal to the streamline n such that

$$Q_c\frac{\partial}{\partial s}=V\frac{\partial}{\partial \rho}+\frac{U}{\rho}\frac{\partial}{\partial \theta}=V_1\frac{\partial}{\partial Y}+U_1\frac{\partial}{\partial X} \tag{27a}$$

$$Q_c\frac{\partial}{\partial n}=-U\frac{\partial}{\partial \rho}+\frac{V}{\rho}\frac{\partial}{\partial \theta}=-U_2\frac{\partial}{\partial Y}+V_2\frac{\partial}{\partial X} \tag{27b}$$

where Q_c is the magnitude of the crossflow velocity, $=\sqrt{U^2+V^2}$ and

$$V_1=VY_\rho+(U/\rho)Y_\theta,\quad U_1=U/\rho \tag{28a}$$

$$U_2=UY_\rho-(V/\rho)Y_\theta,\quad V_2=V/\rho \tag{28b}$$

It follows that

$$Q_c^2\frac{\partial^2}{\partial s^2}=V_1^2\frac{\partial^2}{\partial Y^2}+2U_1V_1\frac{\partial^2}{\partial X\partial Y}+U_1^2\frac{\partial^2}{\partial X^2} \tag{29a}$$

$$Q_c^2\frac{\partial^2}{\partial n^2}=U_2^2\frac{\partial^2}{\partial Y^2}-2U_2V_2\frac{\partial^2}{\partial X\partial Y}+V_2^2\frac{\partial^2}{\partial X^2} \tag{29b}$$

Thus, the principal part of Eq. (26) can be written in terms of local crossflow streamline directions as

$$A_1\frac{\partial^2 F}{\partial X^2}+A_2\frac{\partial^2 F}{\partial X\partial Y}+A_3\frac{\partial^2 F}{\partial Y^2}=(a^2-Q_c^2)\frac{\partial^2 F}{\partial s^2}+a^2\frac{\partial^2 F}{\partial n^2} \tag{30}$$

Equation (30) will be utilized in the numerical solution of Eq. (26).

IV. Numerical Formulation

The numerical solution of Eqs. (21) and (26) with boundary conditions in Eqs. (23-25) are in a suitable form for the application of mixed-flow relaxation procedures which have been so successful for transonic flows. These procedures stem from the work by Murman and Cole[28] for the transonic small disturbance equation. We apply the formulation by Jameson[30] for the transonic full potential equation.

Consider the computational plane shown in Fig. 2. We will be using the notation that a superscript + denotes new values to be computed (for j subscript) or used (for $j+1$ subscript); otherwise values from the previous iteration are used.

All first derivatives are approximated in terms of old values as

$$F_X=(F_{i+1,j}-F_{i-1,j})/2\Delta X \tag{31a}$$

$$F_Y=(F_{i,j+1}-F_{i,j-1})/2\Delta Y \tag{31b}$$

When the crossflow is subsonic $Q_c^2=U^2+V^2<a^2$, the second derivatives are approximated by central differences as follows

$$F_{XX}=\frac{1}{\Delta X^2}(F^+_{i+1,j}-2F^+_{i,j}+F^+_{i-1,j}) \tag{32a}$$

$$F_{XY}=\frac{1}{4\Delta X\Delta Y}(F^+_{i+1,j+1}-F^+_{i-1,j+1}-F_{i+1,j+1}+F_{i-1,j-1}) \tag{32b}$$

$$F_{YY}=\frac{1}{\Delta Y^2}\left(F^+_{i,j+1}-\frac{2}{\omega}F^+_{i,j}-2\left(1-\frac{1}{\omega}\right)F_{i,j}+F_{i,j-1}\right) \tag{32c}$$

where ω is the over-relaxation factor, $0\le\omega<2$.

For the points where the crossflow is supersonic, $Q_c^2=U^2+V^2>a^2$, the principal part of Eq. (26) is written in

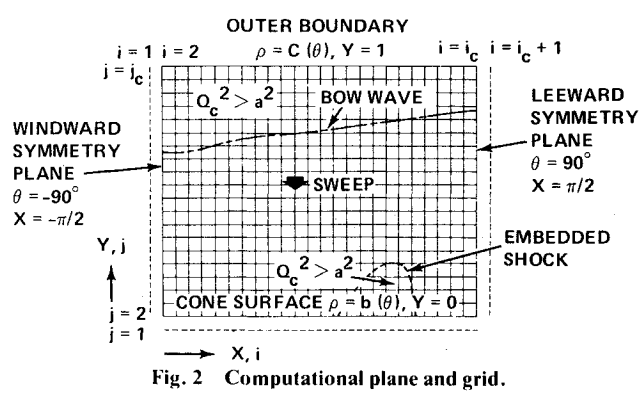

Fig. 2 Computational plane and grid.

terms of the local crossflow streamline coordinates as given by Eq. (30). Contributions to the F_{nn} term, Eqs. (29), utilize central difference expressions identical to Eqs. (32) with the exception of F_{YY} which is approximated by

$$F_{YY}=\frac{1}{\Delta Y^2}\left(F^+_{i,j+1}-F^+_{i,j}-F_{i,j}+F_{i,j-1}\right) \tag{33}$$

Contributions to F_{ss} in Eqs. (29), are approximated by the following backwards difference expressions

$$F_{XX}=\frac{1}{\Delta X^2}\left(2F^+_{i,j}-F_{i,j}-2F^+_{i\mp 1,j}+F_{i\mp 2,j}\right) \tag{34a}$$

$$F_{XY}=\pm\frac{1}{\Delta X\Delta Y}\left(F^+_{i,j+1}-F_{i\mp 1,j+1}-2F^+_{i,j}+F_{i,j}+F^+_{i\mp 1,j}\right) \tag{34b}$$

$$F_{YY}=\frac{1}{\Delta Y^2}\left(2F^+_{i,j}-F_{i,j}-2F^+_{i,j+1}+F_{i,j+2}\right) \tag{34c}$$

where in the double signed expressions the upper sign is used when U_1, Eq. (28), is positive and the lower sign when U_1 is negative.

In addition, in order to insure uniform convergence of the difference scheme for cases where the crossflow Mach number becomes large, it was found necessary to include a temporal artificial viscosity of the form[30]

$$\epsilon\frac{\Delta t}{\Delta Y}\frac{|U_2|}{Q_c}F_{st}$$

where the temporal cross derivative is approximated by

$$F_{st}=\frac{V_1}{Q_c}F_{Yt}+\frac{U_1}{Q_c}F_{Xt}=\frac{V_1}{Q_c\Delta Y\Delta t}\left(F^+_{i,j+1}-F^+_{i,j}-F_{i,j+1}+F_{i,j}\right)$$

$$\pm\frac{U_1}{Q_c\Delta X\Delta t}\left(F^+_{i,j}-F^+_{i\mp 1,j}-F_{i,j}+F_{i\mp 1,j}\right) \tag{35}$$

A stability analysis by Jameson has shown that

$$\epsilon^2>M_L^2-1$$

where M_L is the maximum local Mach number. In practice, values of ϵ from $-5<\epsilon\leq 0$ have been used.

The finite-difference applications of the surface boundary condition are implemented through the use of a dummy row of grid lines below the body at $j=1$, (see Fig. 2). Then, from Eq. (23)

$$F_{i,1}=F_{i,3}-2\Delta Y\left[\frac{db}{d\theta}\left(F_{i+1,2}-F_{i-1,2}\right)/2\Delta X\right.$$

$$\left.+Hb\left(\frac{db}{d\theta}U_\infty-bV_\infty\right)\right]\Big/\left[Y_\rho\left(b^2+\frac{db^2}{d\theta}\right)\right] \tag{36}$$

Now the same finite-difference expressions can be used at the boundary $j=2$ as the interior points.

Similarly, at the symmetry planes $i=2$ and $i=ic$ we introduce dummy columns $i=1$ and $i=ic+1$ and approximate Eq. (24) as

$$F_{1,j}=F_{3,j} \tag{37a}$$

$$F_{ic+1,j}=F_{ic-1,j} \tag{37b}$$

At the outer boundary $j=jc$, $\rho=c(\theta)$, and if c was chosen to be outside the bow wave, then the crossflow will be supersonic and Eqs. (25) imply

$$F_{i,jc}=0 \tag{38a}$$

$$\left(\frac{dF}{dY}\right)_{i,jc}=0 \tag{38d}$$

The preceding finite-difference expressions, Eqs. (31-35), and boundary conditions, Eqs. (36-38), are written in tridiagonal form for values of the correction $F^+_{ij}-F_{ij}$ along rows $j=$constant. These expressions are solved by Gaussian elimination starting with the outer boundary $j=jc$ and sweeping to the body $j=2$. This scheme retains diagonal dominance as long as the grid is swept by no more than 90 deg from the local crossflow streamline direction. In a few cases, such as thin cones at very high angles of attack, this condition was violated. Here we reformulated the difference expressions so that we could march along rows from the outer boundary to a specified row above the body, and then in a consistent fashion to march along columns from the windward symmetry plane to the leeward symmetry plane (see Fig. 2). This procedure produced the necessary diagonal dominance.

The formulation of the relaxation procedure is ideally suited for developing the bow shock since the choice of coordinate grid is nearly in the direction of $Y=$constant and the sweep is nearly normal to the shock. Furthermore, outside the bow shock the conical perturbation potential F should equal zero. Thus, the fact that the integration scheme is first order in the supersonic region should not greatly affect the accuracy of the bow shock solution. Proper computation of the bow wave is critical to the accurate calculation of the entire field including the surface values. In addition, the rotated difference scheme can treat situations where embedded shocks appear near the cone surface. The numerical formulation is also well suited for the computation of nodal and saddle point singularities. These singularities always appear in the vicinity of conical stagnation points and hence in the elliptic portions of the computation. In these regions accurate solutions for the potential function can be obtained independent of the sweep direction.

The preceding numerical formulation of the nonlinear, mixed potential flow boundary-value problem was developed in nonconservation form. For the transonic flow problem, nonconservation form inviscid solutions are known to be less accurate since they develop a mass source at the embedded shocks which tend to displace the streamlines at downstream infinity.[33] It is also known, however, that these nonconservation form solutions give better agreement with data, which is likely fortuitous, and would not be the case with an adequate viscous interaction solution.[34] It is not clear whether the spurious mass source will cause a significant difficulty in the conical flow solutions, since the streamlines downstream of the embedded shock are constrained to end at the conical surface on the leeward generator (the vortical singularity). The present formulation stands on the basis of agreement with other theoretical work and experimental data in the following section.

V. Results

The numerical procedure for relaxation solutions of irrotational conical flows has been applied to a wide variety of cases ranging from slender cones to thin wings with supersonic leading edges at moderate supersonic Mach numbers ranging from 1.2 to 2 and at angles of attack ranging up to 30 deg. First, we will present a number of cases where the conical relaxation solution can be compared with existing analytic methods and wind-tunnel data. In addition, a number of crossflow streamline patterns will be presented, illustrating the "lift-off" of the vortical singularity at high angles of attack on circular and elliptic cones.

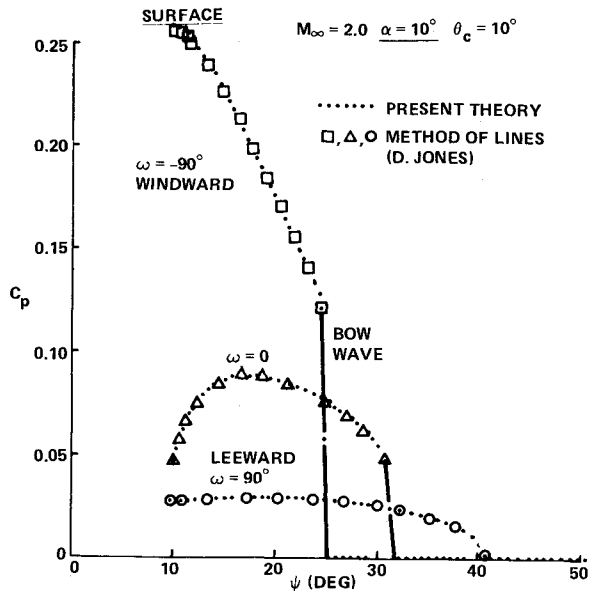

Fig. 3 Shock-layer pressure distribution on a circular cone at incidence. Comparison with method of lines.

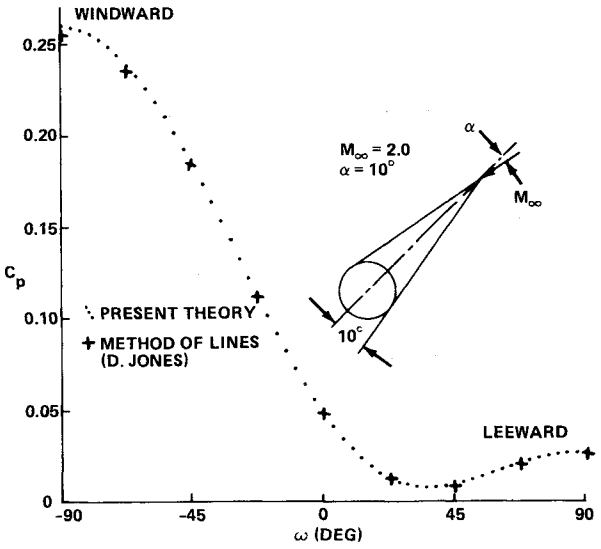

Fig. 4 Surface pressure distribution on a circular cone at incidence. Comparison with method of lines.

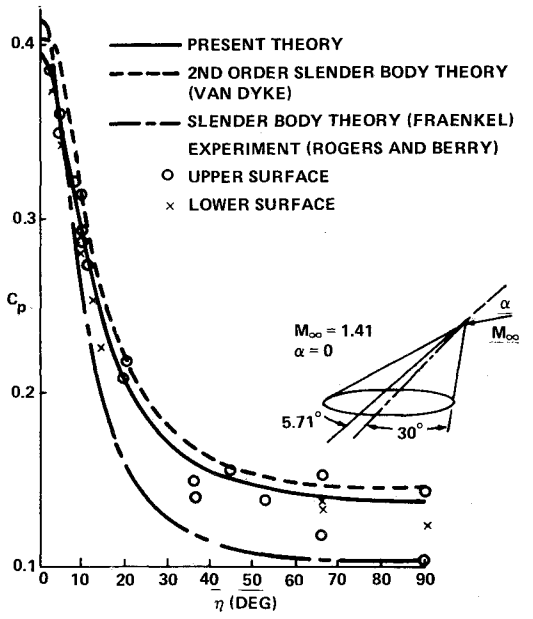

Fig. 5 Surface pressure distribution on an elliptic cone at zero incidence. Comparison with slender body theory.

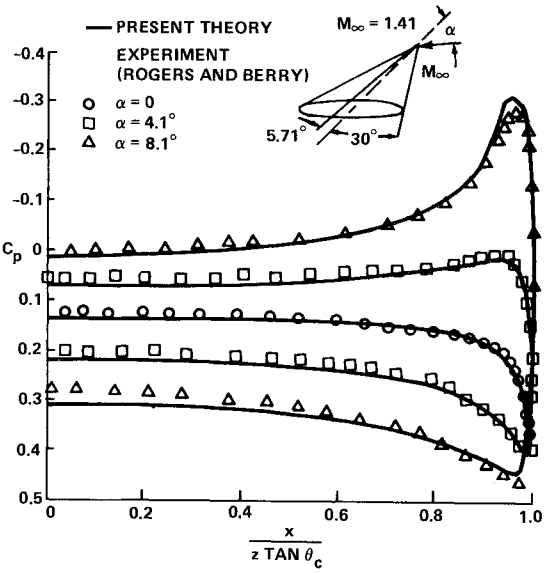

Fig. 6 Surface pressure distribution on an elliptic cone at several values of incidence. Comparison with experimental data.

Before the results are presented some terminology in the figures will be explained. For elliptic cones, the angles θ_c and δ_c refer to the half angle of the cones along the semimajor and semiminor axes, respectively. The eccentricity of the elliptic cone is $E = \tan\theta_c / \tan\delta_c$. The angle ω is -90 deg along the windward symmetry plane and equals $+90$ deg along the leeward symmetry plane. The axis $x/z \tan\theta_c$ is the normalized distance along the span of the wing and is equal to 1 at the leading edge. The angle ψ is the azimuthal angle of a spherical coordinate system centered at the cone apex and measured from the cone centerline.

First we present some solutions for a slender circular cone, half angle 10 deg, $M_\infty = 2.0$ at $\alpha = 10$ deg in Figs. 3 and 4. The conical relaxation results are compared with solutions by Jones[35] using the method of lines. In the method of lines, the flow rotationality is fully accounted for, so these comparisons indicate the effect of the irrotational flow assumption in the present method under these conditions. The agreement in the shock layer, Fig. 3, is excellent, including the position and strength of the bow shock which is smeared over three grid points in the relaxation solution. The surface pressure shown in Fig. 4 is also in excellent agreement.

Next we present the conical relaxation results for an elliptic cone at $M_\infty = 1.41$ and zero incidence. The surface pressure is plotted as a function of the elliptic-conical angle η for the case $\theta_c = 30$ deg, $\delta_c = 5.7106$ deg, $E = 5.77$ in Fig. 5. The angle $\eta = \tan^{-1}(E \tan\omega)$ spreads out the region of steep pressure gradient near the leading edge. Also shown on the plot are the slender body solutions of Fraenkel[5] and Kahane and Solarski,[6] the second-order slender body solution of Van Dyke,[7] and experimental results from Rogers and Berry.[36] The conical relaxation results are in very good agreement with the data and with the second-order slender body result.

The effects of incidence on the surface pressures of two elliptic cones are shown in Figs. 6 and 7 along with more experimental data from Rogers and Berry.[36] The agreement for the cone in the preceding figure, $E = 5.77$, is very good for all values of α shown in Fig. 6. Solutions for a much thinner elliptic cone, $\theta_c = 30$ deg, $\delta_c = 2.8624$ deg, $E = 11.55$ are presented in Fig. 7. For the larger angles of attack on the thin ellipse some discrepancies are noted. At $\alpha = 6.1$ deg, the calculation overpredicts the leading-edge suction, which is

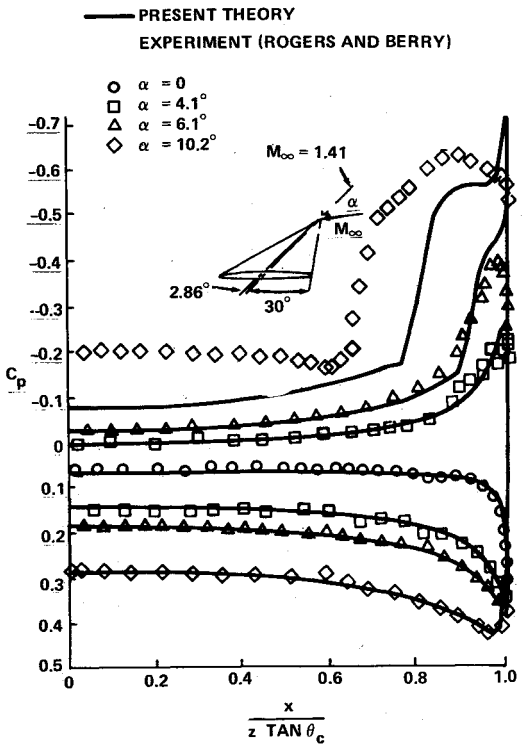

Fig. 7 Surface pressure distribution on a thin elliptic cone at several values of incidence. Comparison with experimental data.

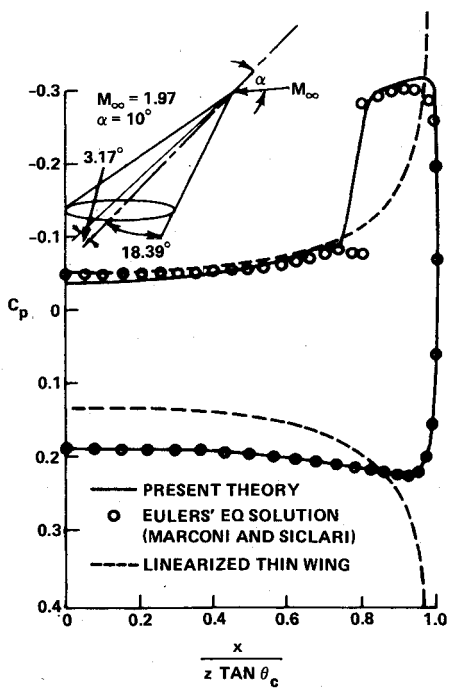

Fig. 8 Surface pressure distribution on an elliptic cone. Comparison with Euler's equations solution.

most probably due to viscous effects; and at $\alpha = 10.2$ a large discrepancy occurs over the entire leeward surface, which can be explained by flow separation. Experimental evidence in terms of shadowgraphs and oil flows in Ref. 36 confirms this.

In order to evaluate the ability of the conical relaxation solution to predict accurately the development of embedded shock waves, we compare our results with recent calculations of Siclari.[37] The technique[22] utilizes explicit marching procedures for the numerical solution of Euler's equations with both the bow shock and crossflow shock explicitly fit to

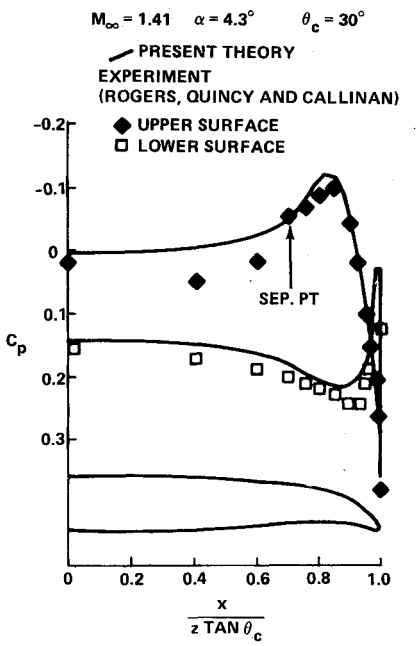

Fig. 9 Surface pressure comparison with data for cambered elliptic cone.

satisfy the Rankine-Hugoniot relations. Figure 8 gives the results for an elliptic cone, $\theta_c = 18.39$, $\delta_c = 3.17$, $E = 6.0$ at $M_\infty = 1.97$ and $\alpha = 10$ deg. The agreement between the two computations is quite good including the position and strength of the embedded shock wave. This gives further support to the applicability of the irrotational flow assumption in the present method. Also shown on the plot is the linearized thin-wing solution (e.g., Jones and Cohen[38]).

To illustrate the ability of our method to handle geometric nonuniformities we present a calculation of a cambered elliptic cone which has been experimentally tested by Rogers et al.[39] This is basically the same cone as shown in Fig. 7 with $\theta_c = 30$ deg and $\delta_c = 2.86$ deg. The camber line was modified outboard of $\bar{x} = x/z\tan\theta_c = 0.7$ by the formula $y/z \tan\theta_c = 4.139\,(0.49 - \bar{x}^2 - 1.4\,\bar{x}\log 0.7/\bar{x})$. The results shown in Fig. 9 are in very good agreement on the windward surface and in the quite complex region near the leading edge. On the inboard portion of the leeward surface flow separation was noticed in the experiment.[39]

The streamline pattern for cones at angles of attack has been computed through a numerical integration of the velocity field after the relaxation solution for the conical potential function has converged. The resulting crossflow streamlines on a slender circular cone are shown in Fig. 10, and for an elliptic cone in Fig. 11. These solutions indicate the character of the conical stagnation points and the development and subsequent lift-off of the vortical singularity from the leeward surface. The crossflow streamline patterns for the circular cone (Fig. 10) confirm the qualitative features of Melnik's analysis[25] based on a local solution. At the low value of $\alpha = 5$ deg the streamlines converge tangential to the cone surface at the leeward nodal point. Next at $\alpha = 10$ deg, or $\alpha/\theta_c = 1$ the streamlines are tending to be normal to the surface of the cone. At the high values of incidence, $\alpha = 20$ deg and $\alpha = 30$ deg, the crossflow becomes supersonic, denoted by the dotted lines, and the vortical singularity lifts off the surface of the cone.

Similar qualitative features of the crossflow streamline pattern occur on the 2:1 elliptic cone in Fig. 11. The minor semiaxis angle of the elliptic cone, $\delta_c = 10$ deg, was the same as the preceding circular cone half angle. The major semiaxis angle was doubled to $\theta_c = 20$ deg. Here, the streamlines at the leeward surface did not become normal to cone surface until $\alpha = 20$ deg or $\alpha/\delta = 2$, $\alpha/\theta_c = 1$. At $\alpha = 30$ deg, the lift-off

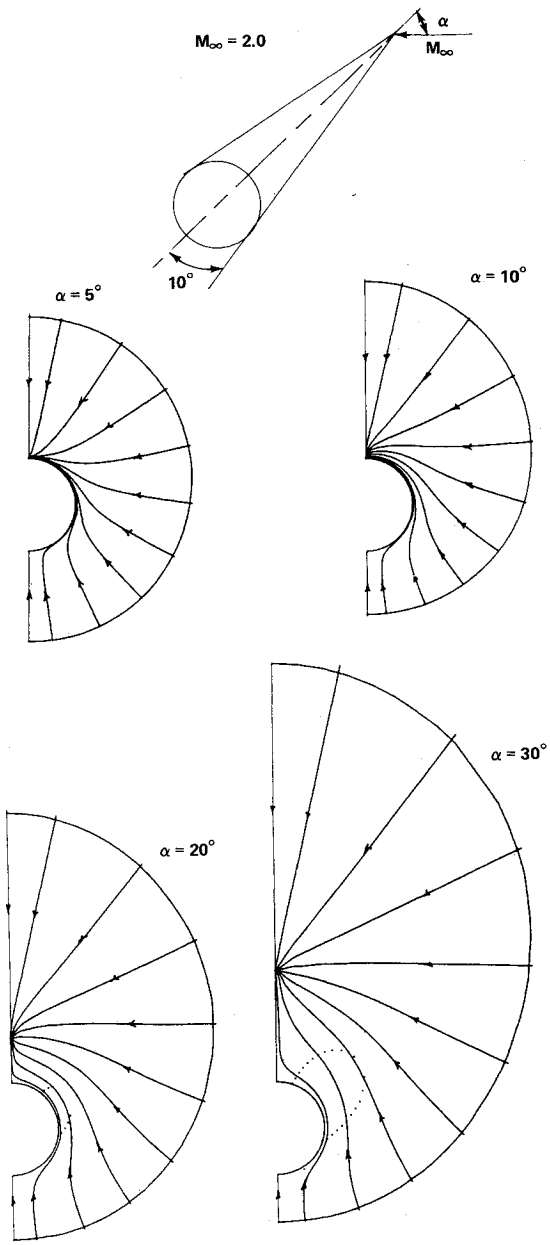

Fig. 10 Crossflow streamline patterns—circular cone.

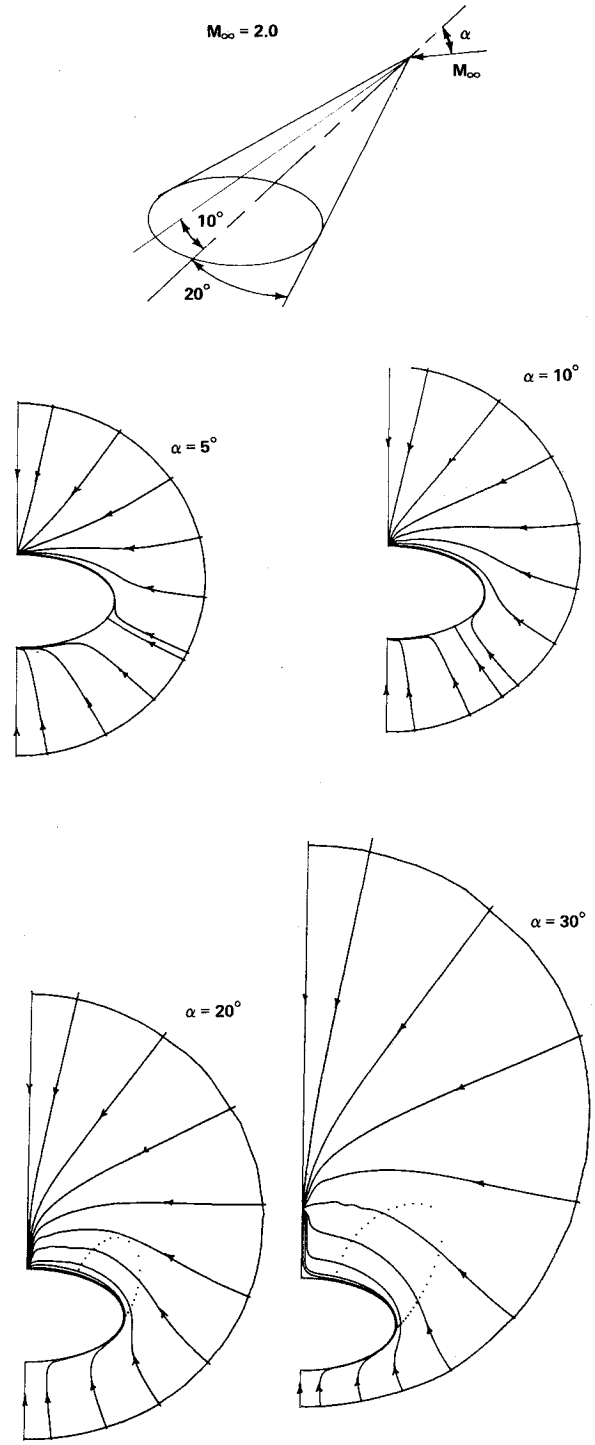

Fig. 11 Crossflow streamline patterns—2:1 elliptic cone.

phenomena can be observed. The movement of the saddle point singularity can be seen to move from near the leading edge at $\alpha = 5$ deg to the windward symmetry plane at $\alpha = 20$ deg. The small oscillations which appear on some of the streamlines in Fig. 11 are a result of the streamline integration routine and not from the numerical relaxation solution of the potential field.

The corresponding surface pressure distribution for the previous two cases are presented in Figs. 12 and 13. The results indicate the effects of incidence and the development of embedded shock waves at large values of incidence on the circular and elliptic cones.

A large variety of other conical flow solutions by the present author are available in Ref. 40. The effects of incidence, Mach number, sweepback, and thickness for thin elliptic cones are described. The conditions include angle of attack up to 20 deg; Mach numbers ranging between 1.25 and 2; sweepback values including subsonic, sonic, and supersonic leading edges; and elliptic cone eccentricities greater than 30:1. Space limitations do not allow the presentation of these results here.

All of the preceding examples in Figs. 3-13 were computed on a sequence of two grids, the finest corresponding to 60 mesh points in the θ direction and 60 mesh points in the ρ direction. Typical numbers of complete iteration cycles were approximately 200 on the coarse grid and 150 on the fine. The computations took from 2-3 min CPU time on the IBM 370/168. Reliable engineering accuracy could be achieved with less stringent convergence tolerance in about 1-2 min CPU time. In addition, various accelerated convergence algorithms recently developed for two-dimensional transonic potential flow problems could serve to further reduce the computation time.

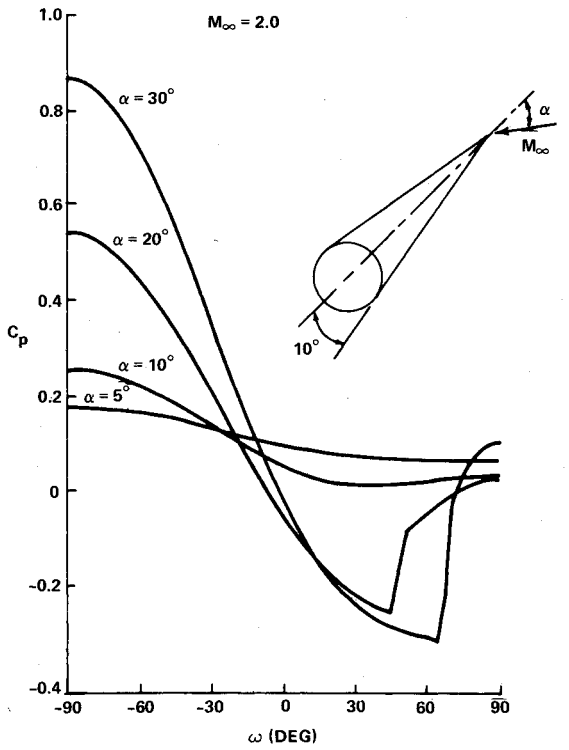

Fig. 12 Angle-of-attack effects on a circular cone.

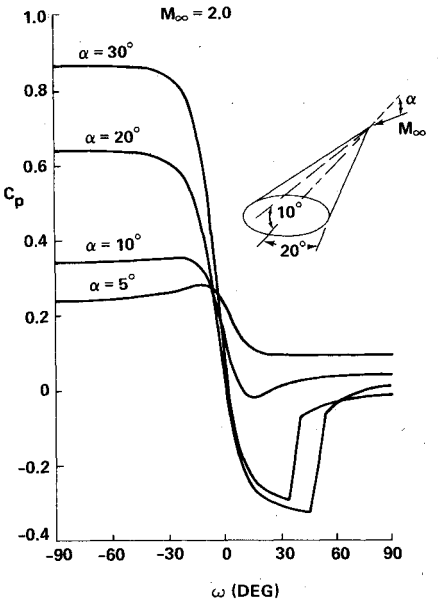

Fig. 13 Angle-of-attack effects on an elliptic cone.

Acknowledgment

The author is indebted to G. daForno of the Engineering Department for suggesting this problem and for his stimulating discussions. The author would also gratefully like to acknowledge the support of A. Jameson of New York University and members of the Research Department including R. E. Melnik, F. Marconi, and M. J. Siclari. This investigation was internally funded with the joint sponsorship of the Advanced Development Organization and the Research Department.

References

[1] von Karman, T. and Moore, N. B., "The Resistance of Slender Bodies Moving with Supersonic Velocities with Special Reference to Projectiles," *Transactions of ASME, Journal of Applied Mechanics*, Vol. 54, 1932, pp. 303-310.

[2] Stewart, H. J., "The Lift of a Delta Wing at Supersonic Speeds," *Quarterly of Applied Mathematics*, Vol. 4, Oct. 1946, pp. 246-254.

[3] Squire, H. B., "An Example in Wing Theory at Supersonic Speed," Aeronautical Research Council, London, England, Reports and Memoranda, No. 2549, 1947.

[4] Ward, G. N., "Supersonic Flow Past Slender Pointed Bodies," *Quarterly Journal of Mechanics and Applied Mathematics*, Vol. 2, 1949, pp. 75-97.

[5] Fraenkel, L. E., "Supersonic Flow Past Slender Bodies of Elliptic Cross Section," Aeronautical Research Council, London, England, Reports and Memoranda, No. 2954, 1952.

[6] Kahane, A. and Solarski, A., "Supersonic Flow About Slender Bodies of Elliptic Cross-Section," *Journal of the Aerospace Sciences*, Vol. 20, Aug. 1953, pp. 513-524.

[7] Van Dyke, M. D., "The Slender Elliptic Cone as a Model for Nonlinear Supersonic Flow Theory," *Journal of Fluid Mechanics*, Vol. 1, May 1956, pp. 1-15.

[8] Adams, M. C., and Sears, W. R., "Slender Body Theory-Review and Extension," *Journal of the Aerospace Sciences*, Vol. 20, Feb. 1953, pp. 85-98.

[9] Wellmann, Von J., "Die Lösung des Anfangsrandwertproblems der linearen Uberschallströmung um einen angestellten Kegel," *Zeitschrift für angewandte Mathematik un Physik*, Vol. 28, 1977, pp. 213-235.

[10] Lighthill, M. J., "The Shock Strength in Supesonic Conical Fields," *Philosophical Magazine*, Vol. 40, 1949, pp. 1202-1223.

[11] Frohn, A., "An Analytic Characteristic Method for Steady Three-Dimensional Isentropic Flow," *Journal of Fluid Mechanics*, Vol. 63, March 1974, pp. 81-96.

[12] Bulakh, B. M., *Nonlinear Conical Gas Flows, (Nelineinye konicheskie techeniia gaza)*, Nauka, Moscow, 1970,

[13] Stone, A. H., "On The Supersonic Flow Past a Slightly Yawing Cone, Part I," *Journal of Mathematics and Physics*, Vol. 27, 1948, pp. 67-81.

[14] Kopal, Z., "Tables of Supersonic Flow Around Cones," MIT, Dept. of Electronics Engineering, Cambridge, Mass., TR-1, 1947.

[15] Ferri, A., "Supersonic Flow Around Circular Cones at Angles of Attack," NACA TN2236, Nov. 1950.

[16] Stocker, P. M. and Mauger, F. E., "Supersonic Flow Past Cones of General Cross Section," *Journal of Fluid Mechanics*, Vol. 13, July 1962, pp. 383-399.

[17] Babenko, K. I., "Investigation of a Three-Dimensional Supersonic Gas Flow Around Conic Bodies," *Proceedings of 11th International Congress of Applied Mechanics*, Munich, Germany, 1964, Springer-Verlag, Berlin, 1966.

[18] Moretti, G., "Inviscid Flow Field Past a Pointed Cone at Angle of Attack, Part I—Analysis," General Applied Sciences Laboratory, Westbury, N.Y., TR No. 577, Dec. 1964.

[19] Jones, D. J., "Numerical Solutions of the Flow Field for Conical Bodies in a Supersonic Stream," National Research Council of Canada Aero. Rept. LR-507, July 1968.

[20] Klunker, E. G., South, J. C., and Davis, R. M., "Calculation of Nonlinear Conical Flows by the Method of Lines," NASA TR R-374, Oct. 1971.

[21] Moretti, G. and Pandolfi, M., "Analysis of the Invsicid Flow About a Yawed Cone, Preliminary Studies," Polytechnic Institute of Brooklyn, PIBAL Rept. No. 72-18, May 1972.

[22] Marconi, F. and Siclari, M. J., "A Study of the Inviscid Flow about Conically Cambered Delta Wings," AIAA Paper 78-58, Jan. 1978.

[23] Kutler, P., "Computation of Three-Dimensional Inviscid Supersonic Flows," *Progress in Numerical Fluid Dynamics, Lecture Notes in Physics*, Vol. 41, Springer-Verlag, Berlin, 1975, pp. 287-374.

[24] Daywitt, J., Anderson, D., and Kutler, P., "Supersonic Flow about Circular Cones at Large Angles of Attack; A Floating Discontinuity Approach," AIAA Paper 77-86, Jan. 1977.

[25] Melnik, R. E., "Vortical Singularities in Conical Flow," *AIAA Journal*, Vol. 5, April 1967, pp. 631-637.

[26] Bakker, P. G. and Bannink, W. J., "Conical Stagnation Points in the Supersonic Flow Around Slender Circular Cones at Incidence," Delft University of Technology, Dept. of Aerospace Engineering, The Netherlands, Rept. VTH-184, Nov. 1974.

[27] Fletcher, C.A.J., "Vortical Singularity behind a Highly Yawed Cone," *AIAA Journal*, Vol. 30, Aug. 1975, pp. 1073-1078.

[28] Murman, E. M. and Cole, J. D., "Calculation of Plane Steady Transonic Flows," *AIAA Journal*, Vol. 9, Jan. 1971, pp. 114-121.

[29] Jameson, A., "Transonic Flow Calculations for Airfoils and Bodies of Revolution," Grumman Aerospace Corporation, Bethpage, N.Y., Aerodynamics Rept. 390-71-1, 1971.

[30] Jameson, A., "Iterative Solution of Transonic Flow Over Airfoils and Wings, Including Flows at Mach 1," *Communication on Pure and Applied Mathematics*, Vol. 27, May 1974, pp. 283-309.

[31] Ives, D. C., "A Modern Look at Conformal Mapping, Including Doubly Connected Regions," AIAA Paper 75-842, June 1975.

[32] Weatherburn, C. E., *Differential Geometry of Three-Dimensions*, Vol. I, University Press, Cambridge, England, 1955, pp. 167-173.

[33] Newman, P. A, and South, J. C., "Conservative vs Non-Conservative Differencing: Transonic Streamline Shape Effects," NASA TMX 72827, 1976.

[34] Melnik, R. E., Chow, R., and Mead, H. R., "Theory of Viscous Transonic Flow Over Airfoils at High Reynolds Number," AIAA Paper 77-680, June 1977.

[35] Jones, D. J., "Tables of Inviscid Supersonic Flow About Circular Cones at Incidence, $\gamma = 1.4$," AGARDograph 137, Pt. I, 1969.

[36] Rogers, E.W.E. and Berry, C. J., "Experiments at $M = 1.41$ on Elliptic Cones with Subsonic Leading Edges," Aeronautical Research Council, Reports and Memoranda, London, England, No. 3042, 1957.

[37] Siclari, M. J., "Investigation of Cross Flow Shocks on Delta Wings in Supersonic Flow," AIAA Paper 79-0345, Jan. 1979.

[38] Jones, R. T. and Cohen, D., *High Speed Wing Theory*, Princeton University Press, Princeton, N.J., 1960, pp. 157, 160.

[39] Rogers, E.W.E, Quincy, V. G., and Callinan, J., "Experiments at $M = 1.41$ on a Thin Conically-Cambered Elliptic Cone of 30° Semi-Vertex Angle," Aeronautical Research Council, Reports and Memoranda, London, England, No. 3306, 1963.

[40] Grossman, B., "A Numerical Procedure for the Computation of Supersonic Conical Flows," AIAA Paper No. 78-1213, July 1978; also available as Grumman Aerospace Corp., Bethpage, N.Y., Research Memorandum RM-658J, Aug. 1978.